Leptogenesis from a feebly interacting dark matter sector

Suresh Chand,[1,*] Mariana Frank,[2,†] and Poulose Poulose[1,‡]
[1]*Department of Physics, Indian Institute of Technology, Guwahati, Assam 781039, India*
[2]*Department of Physics, Concordia University, 7141 Sherbrooke St. West, Montreal, Quebec H4B 1R6, Canada*

(Received 22 April 2022; accepted 18 August 2022; published 30 August 2022)

We perform an analysis of leptogenesis in the context of a simple extension of the Standard Model with two fermions, one charged (χ) and one neutral (ψ), in addition to three right-handed neutrinos, interacting through a charged gauge singlet scalar S. The dark sector (χ and ψ) interacts feebly and produces a relic density consistent with the existing data. The right-handed neutrinos decay into the charged scalar S and a lepton, providing, along with the virtual exchange of S in the standard decay channel, an additional source of CP asymmetry. The advantage of this scenario is that it can generate naturally the observed baryon asymmetry of the Universe, even for right-handed neutrino masses in 10 TeV region, without requiring neutrinos to be degenerate.

DOI: 10.1103/PhysRevD.106.043030

I. INTRODUCTION

Two of the outstanding issues facing the particle physics today are the origin of baryon asymmetry of the Universe (BAU) and finding a suitable Dark Matter (DM) candidate. Expressed in terms of the ratio of the difference between baryon (n_B) and antibaryon ($n_{\bar{B}}$) number densities to the number density of photons in the universe, the BAU as obtained from the cosmic microwave background (CMB) radiation [1] and nucleosynthesis studies (BBN) [2] is

$$\eta = \frac{n_B - n_{\bar{B}}}{n_\gamma} = \begin{cases} (5.8 - 6.6) \times 10^{-10}, & \text{BBN} \\ (6.09 \pm 0.06) \times 10^{-10}, & \text{CMB}. \end{cases} \quad (1.1)$$

In a general framework of elementary particle dynamics, Sakharov [3] showed the particle antiparticle asymmetry can arise dynamically from a charge symmetric or even from an arbitrary initial state and that, to generate BAU, it is necessary to have (i) interactions that violate baryon number (B), (ii) the violation of combined charge conjugation and parity symmetries (CP), and (iii) a departure from thermal equilibrium in the early stages of the Universe when BAU was established. In most particle physics models, the out-of-equilibrium condition is provided by the first-order phase transition of the electroweak symmetry breaking [4–6]. In particular, in the Standard Model (SM), such first-order phase transition requires the Higgs boson to be lighter than its observed mass [7–10].

An alternative mechanism to generate BAU known as leptogenesis [11] was proposed, where a lepton number asymmetry generated in particle interactions is transferred to the baryon number asymmetry. This required lepton number violating processes, along with CP violation and departure from thermodynamic equilibrium, which can be efficiently transformed, in the early stages of the Universe, into the baryon number excess through the so-called sphaleron processes [11–15]. Most neutrino-mass models require the presence of a heavy Majorana neutrino, the decay of which violates lepton number. The necessary CP violation is generated through the quantum corrections of the decay process, which becomes out of equilibrium at a temperature of the order of the mass the decaying particle. In the past few decades, leptogenesis studies were extensively presented in the literature, e.g., [16–31]. The standard leptogenesis scenario with three right-handed Majorana neutrinos added to the SM requires these neutrinos to be heavier than 10^9 GeV [16–19], when the masses are hierarchical, which may be relaxed slightly with the consideration of flavor effects. On the other hand, if the lightest of the additional neutrinos is degenerate in mass with at least one more heavy neutrino, the resonant mechanism can bring in large enough effects even with TeV scale masses for the neutrinos [32,33]. Away from the standard mechanism, there have been many proposals to obtain low-scale leptogenesis [34–43]. In particular, Ref. [43] considers a framework which can address the DM problem along with successfully generating low-scale leptogenesis.

*sures176121102@iitg.ac.in
†mariana.frank@concordia.ca
‡poulose@iitg.ac.in

Regarding the dark matter (DM) problem [44–47], while evidence for dark matter is well established through a variety of cosmological and astrophysical observations, the nature of dark matter remains to be understood. The primary candidate for DM is a new kind of elementary particle. The most popular choice are weakly interacting massive particles (WIMPs), which can explain the observed value of the DM relic density by a mechanism called freeze-out [48]. The assumption underlying thermal freeze-out is that the DM particle is a WIMP that was once in thermodynamic equilibrium with the hot plasma of SM particles created after inflation. As the universe expanded and cooled, when the reaction rate became smaller than the Hubble expansion rate, the DM decoupled and its abundance, known as the relic density, remained the same. This is precisely measured to be $\Omega h^2 = 0.118 \pm 0.001$ [49]. However, extensive s of models with WIMPs ran into difficulties in trying to satisfy both relic density constraints and constraints from direct detection of dark matter experiments [50]. In direct detection, WIMP DM particles could scatter off an atomic nucleus, with observable signals resulting from the recoil of the nucleus. In simple WIMP set ups, this scattering is also controlled by the same coupling and mass parameters that enter the processes controlling the relic density. To avoid WIMP difficulties, other possibilities like the feebly interacting massive particles (FIMPs) were proposed. Unlike for the WIMPs, couplings of FIMPs are too weak to have produced an abundance in thermal equilibrium in the early Universe. Rather, they are slowly produced, in most viable scenarios, through the decay of a partner particle, which itself is in thermal equilibrium to start with. The relic density slowly becomes saturated at the presently observed value, in the so-called freeze-in mechanism [51,52]. The advantage of this scenario is that the couplings are too weak to be of any significance in direct detection experiments, thus evading the limits arising from those. A comprehensive study of freeze-in mechanism was presented in e.g., [53–56], and specifically within baryogenesis, in [57,58].

A previous work [59] presented a model capable of exploring the dark matter problem through freeze-in and freeze-out mechanisms, through an interplay of thermal production with a contribution through the feeble decay of an additional dark fermionic partner. Apart from the fermionic dark matter candidate, the model introduced two charged partners, a fermion and a scalar, with delayed decays leading to the presence of long-lived particles at the LHC. In that scenario, dark matter satisfying experimental constraints can be probed for masses ranging from a few GeV to close to 1 TeV, as opposed to the keV–MeV dark matter mass ranges available in simple FIMP scenarios. In this work we further explore this model, including three Majorana neutrinos, to possibilities for generating leptogenesis. The only modification required here is to treat the Yukawa couplings as nondiagonal to allow for lepton flavor violation. We investigate the additional channels for successful leptogenesis, and show that, in addition to providing a dark matter sector for a wide range of masses, the model can also produce the correct amount of matter antimatter asymmetry with TeV scale Majorana neutrinos. Thus we show that we can achieve low-scale leptogenesis within a consistent FIMP dark matter scenario, without any fine tuning. Through an extensive scan of parameters, we identify simple conditions on Yukawa couplings, consistent with neutrino masses generation and dark matter constraints, for this realization.

Our work is organized as follows. In Sec. II we summarize the model. This is followed by a brief discussion of the dark matter scenario within the FIMP mechanism in this framework in Sec. III, exploring possibilities to generate the correct relic density through two-body decays, in III A or four-body decays, in III B. In Sec. IV, details of generating the leptogenesis in the proposed scenario are presented, and the effect of the new scalar degree of freedom in achieving the required CP asymmetry is established in IV A. We also include explicit Boltzmann equations for time evolution of the number density in nonthermal equilibrium in IV B. Detailed numerical studies and discussion are presented in Sec. V. Finally we summarize our findings and conclude in Sec. VI.

II. A MODEL WITH FIMP DARK MATTER

We thus revisit here the extended model with heavy neutrinos and with additional particles added to spectrum as d in [59]. The extension to the SM particle content includes a gauge singlet charged scalar field S^+, plus one charged (χ^+) and one neutral (ψ) singlet fermions, interacting feebly with the SM particle content. With an additional Z_2 symmetry under which both χ^+ and ψ are odd, while all other particles even, ψ is a stable dark matter candidate. The additional particle spectrum together with their hypercharges and Z_2 charges are given in Table I. Including the above particle content, the Lagrangian of the model is given by

$$\begin{aligned}\mathcal{L}_m = {} & \mathcal{L}_{\rm SM} + (D_\mu S)^\dagger D_\mu S + \bar{\chi}\imath\gamma^\mu D_\mu \chi + \bar{\psi}\imath\gamma^\mu \partial_\mu \psi \\ & + \sum_i \overline{N_i}\,\imath\gamma^\mu \partial_\mu N_i - m_\chi \bar{\chi}\chi - m_\psi \bar{\psi}\psi - \sum_{ij} m_{Nij}\overline{N_i} N_j \\ & - \left(y_1 \bar{\chi} S \psi + \sum_{ij} y_{2ij}\overline{N_i} S l_j + \sum_{ij} Y_{Nij} \bar{L}_i \tilde{\phi} N_j + \text{H.c.} \right) \\ & - (\mu_S^2 S^\dagger S + \lambda (S^\dagger S)^2 + \lambda_1 S^\dagger S \phi^\dagger \phi), \end{aligned} \tag{2.1}$$

where ϕ and $\tilde{\phi} = \imath\sigma_2\phi^*$ represent the SM Higgs doublet, and L_i and l_i denote the SM left-handed lepton doublet and right-handed charged lepton singlet, respectively. The summation indices i, j run from 1 to 3, indicating the three flavors of leptons. Further, we consider hierarchical

TABLE I. Additional fields in the model, together with their hypercharges and Z_2 charges. All fields are $SU(2)_L$ singlets, the neutrinos N_i $(i = 1, 2, 3)$ are Majorana fermions, χ, ψ are vectorlike fermions, and S is a scalar.

Fields	Spin	Y	Z_2
S^+	0	+2	+
N_1, N_2, N_3	$\frac{1}{2}$	0	+
χ^+	$\frac{1}{2}$	+2	−
ψ	$\frac{1}{2}$	0	−

right-handed neutrinos in the basis with $m_N = \mathrm{diag}(m_{N_1}, m_{N_2}, m_{N_3})$.

In the broken electroweak symmetry phase, the vacuum expectation value (VEV) of ϕ, v induces a Dirac mass term through the Yukawa interaction of the right-handed neutrinos to the SM leptons,

$$\mathcal{L}_Y \supset \sum_{ij} m_{Dij}\, \bar{\nu}_{Li} N_j + \mathrm{H.c.}, \tag{2.2}$$

where the Dirac mass matrix is given by $m_D = \frac{v}{\sqrt{2}} Y_N$. This leads to the neutrino mass terms,

$$\mathcal{L}_{\mathrm{mass}} \supset (\bar{\nu}_L \bar{N}) \begin{pmatrix} \mathbf{0} & m_D \\ m_D^T & m_N \end{pmatrix} \begin{pmatrix} \nu_L^c \\ N \end{pmatrix} \tag{2.3}$$

with the Type-I seesaw mechanism [60–65] generating light neutrino masses $m_\nu = m_D^T m_N^{-1} m_D$. The masses of the heavy right-handed neutrinos, on the other hand, remains the same as m_{Ni} with negligible correction, which we ignore. In terms of the mass eigenstates, we have

$$\mathcal{L}_{\mathrm{mass}} \supset \sum_\alpha m_{\nu\alpha}\, \bar{\nu}_{L\alpha} \nu_{L\alpha}^c + \sum_i m_{Ni} \bar{N}_i N_i, \tag{2.4}$$

with the gauge eigenstates of the light neutrinos related to the mass eigenstates through mixing matrix U, known as the Pontecorvo-Maki-Nakagawa-Sakata (PMNS) matrix [66] as

$$\nu_{L\alpha} = \sum_i U_{\alpha i} \nu_{Li}, \tag{2.5}$$

where α indicating the mass eigenstates, while i the flavor eigenstates.

Conversely, from the experimental results on the masses and mixings of the light neutrinos, we can reconstruct Y_N for given heavy neutrino masses. We adopt the Casas-Ibarra parametrization (CI) [67,68] to represent Y_N as

$$Y_N = D_{\sqrt{M}} R\, D_{\sqrt{\kappa}} U^\dagger, \tag{2.6}$$

where $(D_{\sqrt{M}})_{ij} = \sqrt{m_{N_i}}\delta_{ij}$, $(D_{\sqrt{\kappa}})_{ij} = \frac{\sqrt{m_i}}{v}\delta_{ij}$, with m_{N_i} and m_i as the masses of the heavy right-handed neutrinos and the light neutrinos, respectively, and R is any arbitrary complex orthogonal matrix.

The VEV of ϕ also contributes to the mass of the charged singlet scalar yielding

$$m_S^2 = \mu_S^2 + \frac{\lambda_1 v^2}{2}. \tag{2.7}$$

On the other hand, the masses of the dark vectorlike fermions, χ and ψ, arise purely through the parameters in the Lagrangian, m_χ and m_ψ, respectively.

III. FERMIONIC FIMP DARK MATTER

In this scenario, the neutral Z_2-odd fermion, ψ emerges as a dark matter candidate, coupling with other particles solely through its Yukawa interaction with the vectorlike gauge singlet charged fermion χ and the charged scalar S. The charged scalar, on the other hand, decays primarily through $S \to N\ell$ channel, which is controlled by the Yukawa coupling y_2, by requiring the mass hierarchy, $m_S > m_N$ for on shell neutrino N. This, however, can be relaxed to accommodate $m_S < m_N$ so that S decay goes through an off shell neutrino N, $S \to \ell N^* \to \ell\nu\phi$. The χ decay has two possibilities. In the kinematic region with $m_\chi > m_S + m_\psi$, χ decays through $\chi \to \psi S$, whereas for $m_\chi < m_S + m_\psi$ the decay proceeds through, $\chi \to \psi S^* \to \psi N^* \ell \to \psi\ell\nu\phi$, further requiring $m_\chi > m_\phi + m_\psi + m_\ell$. While the two-body decay is controlled by the Yukawa coupling y_1 alone, the other decay is dictated by the combination of $y_1 y_2$. With the corresponding Yukawa couplings combination sufficiently large, the dark matter fermions can be produced copiously as to be in thermal equilibrium in the early stages of the Universe. Then, through the nonequilibrium processes near temperature $T \sim m_\psi$, the annihilation process $(\psi\psi \to SS)$ brings down their number density to eventually satisfy the relic abundance at the decoupling. This requires the mass hierarchy $m_\psi > m_S$. On the other hand, if the relevant coupling combination is much weaker, the production process $\chi \to \psi + \cdots$ can be sufficiently slow to enable the FIMP mechanism to generate the required dark matter abundance.

Viability of all the above scenarios are studied in Ref. [59], treating the Yukawa couplings y_2 as well as Y_N diagonal. Relaxing this requirement to include nonzero off-diagonal couplings in both cases is necessary to generate leptogenesis. This is the focus of the present work, where we explore the parameter space that could accommodate the required relic density. The off-diagonal couplings induce lepton flavor violation (LFV) through Y_N as well as y_2. Since Y_N is involved in the seesaw mechanism, it is naturally required to be small. Furthermore, we shall restrict our s to the case where $y_2 \ll 1$, to avoid inducing large LFV. Thus in our model the LFV is negligibly small.

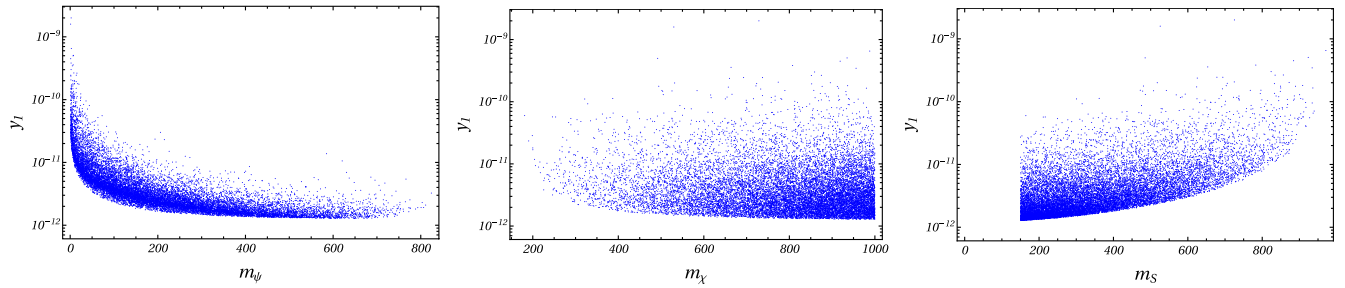

FIG. 1. Yukawa coupling y_1 as a function of the masses of the dark matter m_ψ (left panel), the charged fermionic partner particle m_χ (middle panel) and the charged scalar m_S (right panel), from the two-body decay.

A. Freeze-in via two-body decay of χ

When the couplings involving the dark matter particle are very small, we may envisage a scenario where the initial number density of dark matter particle is negligible, and the observed abundance of dark matter is produced by the slow decay of the partner particles. In this case, the process could occur through the slow decay of $\chi \to S + \psi$ if kinematically allowed ($m_\chi > m_S + m_\psi$), and will continue until the Universe cools down to temperature $T < m_\chi$. Below this temperature, due to the Boltzmann suppression of the number density of χ ($n_\chi \propto \exp(-m_\chi/T)$), there is no further addition to the number density of the dark matter fermion ψ, leading to a constant comoving number density. This mechanism of generating the dark matter relic density is known in the literature as the freeze-in mechanism. Since the initial DM number density is negligible, the inverse decay is irrelevant, and the Boltzmann equation satisfied by the dark matter particle is given by

$$\frac{dY_\chi}{dz} = \frac{2Y_\chi^{\rm eq}}{zH}\frac{K_1(z)}{K_2(z)}\Gamma_{\chi\to S\psi}, \tag{3.1}$$

leading to the relic density, [52]

$$\Omega h^2 = \frac{2.19\times 10^{27} g_\chi}{g_*^S\sqrt{g_*^\rho}}\frac{m_\psi \Gamma_{\chi\to S\psi}}{m_\chi^2}. \tag{3.2}$$

With the Lagrangian in Eq. (2.1), the decay width becomes, in terms of the masses of the particles involved and the Yukawa coupling y_1

$$\Gamma_{\chi\to S\psi} = \frac{y_1^2}{16\pi m_\chi^3}[(m_\chi + m_\psi)^2 - m_S^2] \times [(m_\chi^2 - m_S^2 - m_\psi^2)^2 - 4m_S^2 m_\psi^2]^{\frac{1}{2}}. \tag{3.3}$$

Putting Eq. (3.3) back into Eq. (3.2), and demanding Ωh^2 to satisfy the observed relic density, the coupling y_1 can be constrained, for given masses of the dark matter and the partner particles. Notice that, in this scenario, the dark matter sector is decoupled from the neutrino sector and does not contribute to leptogenesis. Within this scenario, selecting the relic density to satisfy the observed value of $\Omega h^2 = 0.118 \pm 0.001$ [49], we scanned the parameter space spanned by the masses m_χ, m_ψ, and m_S to obtain the value of the coupling y_1 obeying the kinematic restriction for the decay, $m_\chi > m_S + m_\psi$. Focusing on light dark matter, and sub-TeV partner particles, we scanned over the parameter range as given in Table II. Allowed values of the parameter space arising from the scan are presented in different planes in Fig. 1. The parameter m_S affects the relic density purely through the phase-space factor, and thus has a clear correlation with the couplings. On the other hand, m_χ is expected to have an anticorrelation effect, considering the dependence of the coupling and the mass of the decaying particle. This is indeed consistent with the plots in Fig. 1. However, the effect is somewhat subdued owing to the additional inverse dependence of the relic density on m_χ. In the case of the dark matter mass, the direct dependence of the relic density on the combination $m_\psi y_1^2$, where the coupling is coming from the decay width, yields a parabolic dependence between the two parameters. The influence of the phase-space factor is weak, as indicated by the spread of the points in the scan. We verified that the width of χ in this parameter range varies between 10^{-25} GeV and 10^{-21} GeV. The charged scalar would decay through $S \to N\ell$, if kinematically allowed. However, as we shall consider the mass of the heavy neutrinos m_N to be in the range of 10 TeV or more, the two-body decay is disallowed. The three-body decay that follows through the heavily off shell neutrino N, along with the Yukawa coupling required for the seesaw

TABLE II. Range of the masses in GeV, scanned to fix the coupling y_1 satisfying the observed relic density.

m_χ	150–1000
m_S	150–1000
m_ψ	1–850

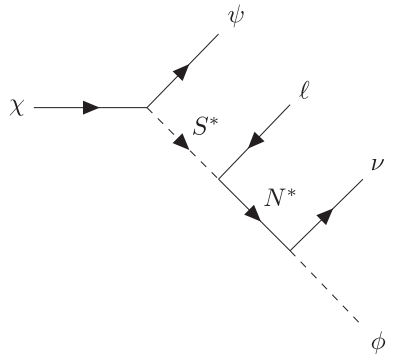

FIG. 2. Feynman diagrams for the χ decay when $m_\phi + m_\psi < m_\chi < m_S + m_\psi$.

mechanism being in the range of 10^{-8} slows down the decay of S. For the parameters considered here, the decay width is in the range of 10^{-24} to 10^{-19} GeV for m_S between 100 GeV and 1 TeV.

B. Freeze-in via four-body decay of χ

In the kinematic region where $m_\chi < m_S + m_\psi$, the two-body decay discussed above is kinematically disallowed. Noting that we are working with $m_S \ll m_N$, the leading allowed decay channel is the four-body decay shown in Fig. 2. This involves the couplings, y_1, y_2 and Y_N. With $m_N \sim 10$ TeV, values of Y_N in the range of 10^{-8} to satisfy the seesaw condition the cross section for this process will require larger y_1 values. For consistency with the parameters chosen from leptogenesis, as discussed in Sec. IV, we restrict y_2 in the range of 10^{-3}–10^{-1}. With these restrictions, we scanned over the masses (m_χ, m_S, m_ψ) and used Eq. (3.2) replacing $\Gamma_{\chi\to S\psi}$ by the four-body width $\Gamma_{\chi\to\ell\nu\phi\psi}$, to obtain y_1 corresponding to the observed relic density. The scan range is as shown in Table II with the additional condition that $m_\chi < m_S + m_\psi$. The resulting parameter space points, projected on to $y_1 - m_i$ plane, where $i = \chi$, S, ψ, are presented in Fig. 3. Clearly, values of y_1 in the range of 10^{-4} are compatible with the dark matter observations.

IV. LEPTOGENESIS

We move on to the analysis of leptogenesis in the scenario considered here, where the necessary lepton number violation and CP asymmetry are generated through the decay of one of the Majorana neutrinos present. In the standard scenario, leptogenesis is generated by the decay of neutrinos through the Higgs doublet, whereas in the scenario presented here, additional possibilities open through the Yukawa interaction term $y_{2ij}\bar{\ell}_i N_j S + \text{H.c.}$ First, $N \to S\ell$ and its CP-conjugate process provide new decay channels. Second, the self-energy and vertex corrections in each of the decays receive additional contributions.We now investigate possibilities in the low-energy leptogenesis enabled by these new interactions.

A. CP asymmetry

As in the standard leptogenesis, the CP asymmetry arises through the interference of the tree-level and the one-loop channels. We denote the CP-violating parameter arising from the standard process involving the Higgs boson as

$$\epsilon_1 = \frac{\Gamma(N_1 \to L\phi) - \Gamma(N_1 \to \bar{L}\,\bar{\phi})}{\Gamma(N_1 \to L\phi) + \Gamma(N_1 \to \bar{L}\,\bar{\phi})}, \tag{4.1}$$

and the corresponding parameter arising from the decay involving the new charged singlet scalar as

$$\epsilon_2 = \frac{\Gamma(N_1 \to \ell S) - \Gamma(N_1 \to \bar{\ell}\,\bar{S})}{\Gamma(N_1 \to \ell S) + \Gamma(N_1 \to \bar{\ell}\,\bar{S})}. \tag{4.2}$$

Figure 4 shows the relevant one-loop diagrams involving the vertex corrections as well as the self-energy corrections. The CP-violating parameters in Eqs. (4.1) and (4.2) can be written explicitly in terms of the self-energy ($\epsilon^{s\xi}$) and vertex contributions ($\epsilon^{v\xi}$), with $\xi = \phi, S$, as

$$\epsilon_1 = \epsilon^{s\phi} + \epsilon^{v\phi}, \tag{4.3}$$

$$\epsilon_2 = \epsilon^{sS} + \epsilon^{vS}, \tag{4.4}$$

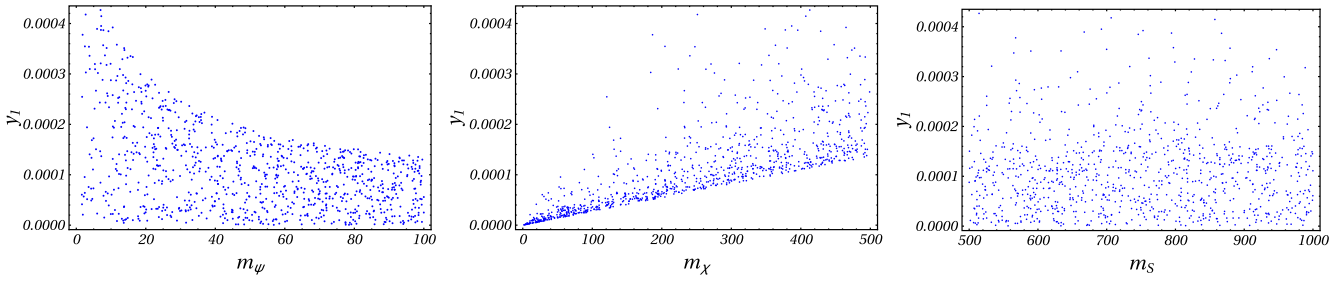

FIG. 3. Yukawa coupling y_1 values versus the mass of non-SM particles, m_ψ (left panel), m_χ (middle panel) and m_S (right panel), from the requirement that they satisfy the relic density bound, from the four-body decay.

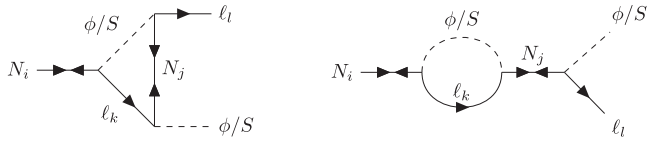

FIG. 4. Feynman diagram corresponding to one loop vertex and self-energy corrections to $N_i \to \ell_l \phi/S$.

where

$$\epsilon^{s\phi} = \frac{1}{8\pi K_{11}} \sum_{j=2,3} \left[\frac{m_{N_1}}{m_{N_1}^2 - m_{N_j}^2} \mathrm{Im}(m_{N_j} K_{1j}^2 + m_{N_1} \kappa_{1j} K_{1j} + m_{N_j} \kappa_{j1} K_{1j}) \right], \tag{4.5}$$

$$\epsilon^{sS} = \frac{1}{8\pi \kappa_{11}} \sum_{j=2,3} \left[\frac{m_{N_1}}{m_{N_1}^2 - m_{N_j}^2} \mathrm{Im}(m_{N_j} \kappa_{j1}^2 + m_{N_1} K_{1j} \kappa_{j1} + m_{N_j} K_{j1} \kappa_{j1}) \right], \tag{4.6}$$

$$\epsilon^{v\phi} = \frac{1}{8\pi K_{11}} \sum_{j=2,3} \mathrm{Im}(K_{1j}^2) \mathcal{F}\left(\frac{m_{N_j}^2}{m_{N_1}^2}\right), \tag{4.7}$$

$$\epsilon^{vS} = \frac{1}{8\pi \kappa_{11}} \sum_{j=2,3} \mathrm{Im}(\kappa_{j1}^2) \mathcal{F}\left(\frac{m_{N_j}^2}{m_{N_1}^2}\right), \tag{4.8}$$

where $\mathcal{F}(x) = \sqrt{x}[1 + (1+x)\ln\frac{x}{1+x}]$, and we have defined the relevant product of the Yukawa couplings as $K_{ij} = (Y_N^\dagger Y_N)_{ij}$ and $\kappa_{ij} = (y_2^\dagger y_2)_{ij}$. Unlike Y_N, the Yukawa coupling combination κ_{ij} connecting $N\ell S$ do not play any role in the seesaw mechanism, but may influence the lepton flavor violating processes, as previously discussed. We shall therefore keep these couplings not larger than of order of 0.1, but otherwise unrestricted. Note that the standard leptogenesis is recovered in the limit $\kappa_{ij} \to 0$, when only the first terms in Eqs. (4.5) and (4.7) survive.

B. The Boltzmann equations

The time evolution of the number density when out-of-thermal equilibrium is obtained using the Boltzmann equations. With $M_{N_3} \gg M_{N_2} \gg M_{N_1}$, any lepton asymmetry generated by the decay of N_2 and N_3 at high temperature is washed out before the electroweak symmetry breaking and the surviving lepton asymmetry is generated by the decay of the lightest right-handed neutrino (N_1). The number of density of N_1 depends on its decay, inverse decay, and scattering process. In the present setup, the following are the relevant processes

(1) Decays: $N_1 \to \phi L, N_1 \to \bar{\phi}\bar{L}, N_1 \to S\ell, N_1 \to \bar{S}\bar{\ell}$;
(2) Inverse decays: $\phi L \to N_1, \bar{\phi}\bar{L} \to N_1, S\ell \to N_1, \bar{S}\bar{\ell} \to N_1$;
(3) Scattering processes:
standard $\Delta L = 1$ s-channel processes: $\ell N_1 \to d\bar{u}$, $\bar{\ell} N_1 \to \bar{d}u$;
standard $\Delta L = 1$ t-channel processes: $N_1 u \to d\bar{\ell}$, $N_1 \bar{u} \to \bar{d}\ell$, $N_1 d \to u\ell$, $N_1 \bar{d} \to \bar{u}\bar{\ell}$;
standard $\Delta L = 1$ processes involving gauge boson A: $N_1 \phi \to AL$, $N_1 A \to \phi L$;
new $\Delta L = 1$ processes involving S: $N_1 \ell \to S\phi$, $N_1 \bar{\ell} \to \bar{S}\bar{\phi}$;
new $\Delta L = 1$ processes involving χ, ψ: $N_1 \ell \to \chi\psi$, $N_1 \bar{\ell} \to \bar{\chi}\bar{\psi}$.

Lepton number asymmetry is induced by all the above processes, and in addition, induced also by the $\Delta L = 2$ processes below:

(4) Standard $\Delta L = 2$ processes: $\ell\ell \to \bar{\phi}\bar{\phi}$, $\phi\ell \to \bar{\phi}\bar{\ell}$;
(5) New $\Delta L = 2$ processes: $S\ell \to \bar{S}\bar{\ell}$, $\phi\ell \to \bar{\ell}\bar{S}$, $\bar{\phi}\bar{\ell} \to \ell S$.

As standard practice, we consider the evolution of the number density normalized by the entropy density, denoted by Y_{N_1} and the effective lepton number density, $Y_L = Y_\ell - Y_{\bar{\ell}}$. Within this framework the Boltzmann equations can be written in the following form,

$$\frac{dY_{N_1}}{dz} = D(-Y_{N_1} + Y_{N_1}^{\mathrm{eq}}), \tag{4.9}$$

$$\frac{dY_L}{dz} = \left(\frac{\epsilon_1 \Gamma_{D_1} + \epsilon_2 \Gamma_{D_2}}{Hsz\, Y_{N_1}^{\mathrm{eq}}}\right)(-Y_{N_1} + Y_{N_1}^{\mathrm{eq}}) - S Y_L, \tag{4.10}$$

where

$$D = \frac{\Gamma_{D_1} + \Gamma_{D_2}}{Hsz\, Y_{N_1}^{\mathrm{eq}}} + S_N. \tag{4.11}$$

$$S_N = \frac{1}{Hsz\, Y_{N_1}^{\mathrm{eq}}} \left[\Gamma_{s_1} + \Gamma_{s_2} + \frac{1}{2}(\Gamma_{s_3} + \Gamma_{s_4} + \Gamma_{s_5} + \Gamma_{s_6}) + 2\Gamma_{s_{\mathrm{new1}}} + 2\Gamma_{s_{\mathrm{new2}}} \right], \tag{4.12}$$

$$S = \frac{\Gamma_{D_1} + \Gamma_{D_2} + 2\Gamma_{st}}{2Hsz\, Y_L^{\mathrm{eq}}} + \frac{S_N Y_{N_1}}{2Y_L^{\mathrm{eq}}}. \tag{4.13}$$

Here Γ_{D_1} and Γ_{D_2} are thermal averaged partial decay widths of $N_1 \to \phi L$ and $N_1 \to S\ell$, respectively, with

$$\Gamma_{D_i}(N_1 \to ab) = \int d\Pi_{N_1} e^{\frac{-E_{N_1}}{T}} \int d\Pi_a\, d\Pi_b (2\pi)^4 \delta^4 \times (P_N - P_a - P_b)|\mathcal{M}(N_1 \to ab)|^2,$$

where $d\Pi_i = d^3P_i/((2\pi)^3\, 2E_i)$, and $\mathcal{M}$ is the corresponding invariant amplitude. The thermal averaged scattering cross sections of the $\Delta L = 1$ standard processes $\ell N_1 \to d\bar{u}$, $\ell N_1 \to \phi A$, $N_1 u \to d\bar{\ell}$, $N_1 d \to u\ell$, $N_1\phi \to AL$, $N_1 A \to \phi L$ are denoted by $\Gamma_{si}, i = 1, \ldots, 6$, respectively, and the corresponding processes involving new particles, $N_1\ell \to \chi\psi$ and $N_1\ell \to S\phi$ are denoted by $\Gamma_{s_{\text{new1}}}$ and $\Gamma_{s_{\text{new2}}}$, respectively. In the case of $\Delta L = 2$ processes listed above, the thermal averaged scattering cross section is jointly denoted by Γ_{st}. In terms of the scattering cross section $\sigma(s)$ with a fixed centre of mass energy $\sqrt{s}$, the thermal averaged cross section is given by [18]

$$\Gamma_{si}(X + a \to 1 + 2) = \frac{T}{64\pi^4} \int_{s_{\min}}^{\infty} ds\, s^{1/2} \hat{\sigma}(s)\, \mathrm{K}_1\left(\frac{\sqrt{s}}{T}\right),$$

Where $\hat{\sigma} \equiv 2s\lambda[1, m_N^2/s, m_a^2/s]\sigma$ is the 'reduced cross section', $\lambda(x, y, z) = (x - y - z)^2 - 4yz$, and $K_1(x)$ is the modified Bessel function of second kind.

Formally, we can write the solutions of Eqs. (4.9) and (4.10) in integral form as

$$Y_{N_1} = e^{-\int Ddz}\left(\int Y_{N_1}^{\text{eq}}\, D\, e^{\int Ddz} dz' + \text{const}\right), \quad (4.14)$$

$$Y_L = \epsilon_1\zeta_1 + \epsilon_2\zeta_2, \quad (4.15)$$

where the efficiency factors ζ_i are given by

$$\zeta_i = e^{-\int Sdz}\left\{\int \frac{\Gamma_{D_i}}{Hsz\, Y_{N_1}^{\text{eq}}}\left[-e^{-\int Ddz}\left(\int Y_{N_1}^{\text{eq}}\, D\, e^{\int Ddz} dz'\right) + Y_{N_1}^{\text{eq}} + \text{const}\right] e^{\int Sdz} dz'' + \text{const}'\right\}. \quad (4.16)$$

Notice that the CP-asymmetry parameter ϵ_1 and the corresponding efficiency factor ζ_1 yield the standard contribution to the lepton number asymmetry, while ϵ_2 and ζ_2 add to the lepton number asymmetry arising through the new dynamics. As expected, in the case of hierarchical right-handed neutrinos with TeV scale masses, the contributions from the standard processes are negligible. We shall explore the parameter region of the model considered where this deficit is compensated by the contribution from the new channels.

V. NUMERICAL ANALYSIS

In this section, we perform the numerical analysis for the lepton asymmetry generated through a combination of CP asymmetry arising through the standard decay and the decay to the newly introduced charged scalar, as well as considering the influence of the washout effect arising through different scattering processes mentioned in Sec. IV B. The CP parameters depend on the coupling constants Y_N and y_2, where, as we noted before, Y_N is constrained by the light neutrino masses and mixings, whereas y_2 is largely unconstrained. Considering the CI parametrization as in Eq. (2.6), Y_N depends on the masses and mixing matrix elements of the light neutrinos, on the masses of the heavy neutrinos, and on the elements of an arbitrary orthogonal matrix, R. We assume normal hierarchy in the light neutrino sector, with the lightest neutrino taken to be massless, and the other two masses set in agreement with constraints from the neutrino oscillation experiments [66,69]. Accordingly, we chose $m_1 = 0$ eV, $m_2 = 0.0083$ eV and $m_3 = 0.051$ eV. The complex orthogonal matrix, R is parametrized as

$$R = \begin{pmatrix} \cos\theta & \sin\theta & 0 \\ -\sin\theta & \cos\theta & 0 \\ 0 & 0 & 1 \end{pmatrix},$$

with θ complex. We scan over the heavy neutrino masses keeping the normal hierarchy $m_{N_1} \ll m_{N_2} \ll m_{N_3}$, with the lightest mass in the 1–100 TeV range, and the heavier ones differing from it by at least one order of magnitude. The dependence of Y_N and y_2 enter the CP asymmetries through their combination K_{1j} and κ_{1j} with $j = 2, 3$, respectively, as given in Eqs. (4.5)–(4.8). The complex nature of these parameters is important in determining the amount of CP violation.

First we consider K_{1j}. With the standard Yukawa couplings given by the CI parametrization as in Eq. (2.6),

$$K_{1j} = (Y_N)^*_{k1}(Y_N)_{kj} = \sum_{k,\alpha,\beta} m_{N_k} \frac{\sqrt{m_\alpha m_\beta}}{v^2} R^*_{k\alpha} R_{k\beta} U_{1\alpha} U^*_{j\beta}, \quad (5.1)$$

which, for the structure of R and the choice of $m_1 = 0$, takes a simpler form,

$$K_{1j} = \frac{m_{N_1} m_2}{v^2}|R_{12}|^2 U_{12} U^*_{j2} + \frac{m_{N_2} m_2}{v^2}|R_{22}|^2 U_{12} U^*_{j2} + \frac{m_{N_3} m_3}{v^2} U_{13} U^*_{j3}. \quad (5.2)$$

Thus, any phase of the elements of R is irrelevant, and we can consider it a real orthogonal matrix. Taking U as the

PMNS matrix [66], the only phases that enter in K_{12} are those of U_{13} and U_{22}, while in K_{13} the phases of U_{13} and U_{32} give rise to the relevant CP phase. However, noticing that for the hierarchical case considered in the heavy neutrino sector, the third term, proportional to M_{N_3}, dominates over the others, the relevant phase in both K_{12} and K_{13} is that of U_{13}. We write this as

$$K_{12} \sim \frac{m_{N_3} m_3}{v^2} \sin\theta_{23} \cos\theta_{13}\ \sin\theta_{13}\, e^{-i\delta_{CP}},$$
$$K_{13} \sim \frac{m_{N_3} m_3}{v^2} \cos\theta_{23} \cos\theta_{13}\ \sin\theta_{13}\, e^{-i\delta_{CP}}, \tag{5.3}$$

while the real matrix element K_{11} can be written as

$$K_{11} \sim \frac{m_{N_3} m_3}{v^2} \sin^2\theta_{13}. \tag{5.4}$$

We use the present experimental values for the mixing angles and the δ_{CP} parameter [69]

$$\theta_{13} = 8.57^{\circ}{}^{+0.13}_{-0.12}, \qquad \theta_{23} = 49.0^{\circ}{}^{+1.1}_{-1.4}, \qquad \delta_{CP} = 195^{\circ}{}^{+51}_{-25}. \tag{5.5}$$

Taking $m_{N_3} \sim 10^3$ TeV, we have $K_{1j} \sim 10^{-8}$. The standard contribution to the self-energy term in the CP-violating parameter can then be read from Eq. (4.5) as

$$\epsilon^{s\phi}_{\rm std} = \frac{1}{8\pi K_{11}} \left[\frac{m_{N_1}}{m_{N_2}} \mathrm{Im}(K_{12}^2) + \frac{m_{N_1}}{m_{N_3}} \mathrm{Im}(K_{13}^2) \right]$$
$$\sim \frac{1}{8\pi K_{11}} \frac{m_{N_1}}{m_{N_2}} \mathrm{Im}(K_{12}^2) \tag{5.6}$$

and the new contribution to the standard decay channel is dominantly

$$\epsilon^{s\phi}_{\rm new} \sim \frac{1}{8\pi K_{11}} \frac{m_{N_1}}{m_{N_2}} \mathrm{Im}(\kappa_{21} K_{12}). \tag{5.7}$$

With a suitably chosen κ_{21}, it may then be possible to lift up the CP-violating parameter to the value required in leptogenesis, even when the standard contribution is a few orders of magnitude smaller. In addition, there is an effect from the new decay channel $N_1 \to \ell S$, which contributes to the self-energy (Eq. (4.6)),

$$\epsilon^{sS} \sim \frac{1}{8\pi\kappa_{11}} \frac{m_{N_1}}{m_{N_2}} \mathrm{Im}(\kappa_{21}^2). \tag{5.8}$$

Notice that the contribution to the standard channel from the virtual effects of the new scalar particle, S is present even if κ_{21} is real, whereas the contribution coming from the new channel is subdominant in this case, as this will now be

$$\epsilon^{sS} \sim \frac{1}{8\pi\kappa_{11}} \frac{m_{N_1}}{m_{N_2}} \mathrm{Im}(\kappa_{21} K_{21}). \tag{5.9}$$

If κ_{1j} is real, the effect of S is completely absent in the vertex correction contribution to the CP-violating parameter, Eqs. (4.7) and (4.8). However, once κ_{1j} has an imaginary part, it could be suitably chosen to get the required CP asymmetry, which now has a dominant contribution from the new scalar S

$$\epsilon^{vS} \sim \frac{1}{8\pi\kappa_{11}} \frac{m_{N_3}}{m_{N_1}} \mathrm{Im}(\kappa_{31}^2). \tag{5.10}$$

As it is proportional to m_{N_3}, the vertex contribution dominates over the self-energy contribution for κ_{1j} of the same order. With these considerations, we now undertake the numerical analysis, scanning the parameter space to find regions that are compatible with the observed baryon asymmetry. We consider four distinct possibilities for κ_{1j}, i.e.,

(1) Real and positive κ_{1j};
(2) Real and negative κ_{1j};
(3) Imaginary and negative κ_{1j};
(4) Complex κ_{1j} with a negative imaginary part.

The signs are chosen so that in each situation we get the correct sign for the CP asymmetry, and these are the only viable scenarios for leptogenesis in our model. Throughout our analysis, we allow the right handed neutrino masses to vary in order to clearly understand the influence of the

TABLE III. The possible leptogenesis scenarios, yielding correct signs for the CP asymmetry, the limits on the couplings, and range of variation for neutrino masses for the asymmetry parameters for each case.

$m_\chi = 200$ GeV, $m_S = 175$ GeV, $m_\psi = 60$ GeV, $10^{-4} \le \kappa_{11} \le 10^{-1}$					
		Couplings	Mass of heavy neutrinos		
Scenario		κ_{12}, κ_{13}	m_{N_1} (TeV)	m_{N_2} (TeV)	m_{N_3} (TeV)
Case 1	Real positive κ	$10^{-3} \le \kappa_{1j} \le 10^{-1}$	(10, 100)	$(10^3, 10^4)$	$(10^5, 10^6)$
Case 2	Real negative κ	$-10^{-1} \le \kappa_{1j} \le -10^{-3}$			
Case 3	Imaginary κ	$-\iota 10^{-3} \le \kappa_{1j} \le -\iota 10^{-1}$			
Case 4	Complex κ	$(1-\iota)10^{-3} \le \kappa_{1j} \le (1-\iota)10^{-1}$			

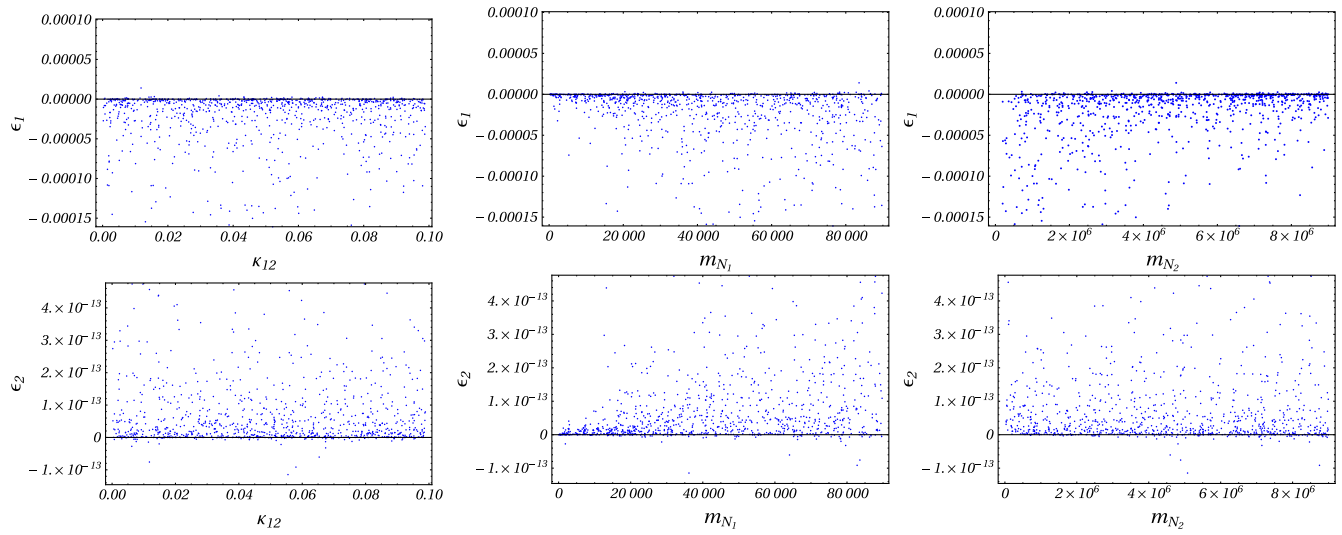

FIG. 5. *CP* asymmetry against the relevant coupling κ_{12} (left panels) and the masses, m_{N_1} (middle panels) and m_{N_2} (right panels) for Case 1, with real κ and masses m_{N_j} in GeV. Top panels: Variation of ϵ_1 with κ_{12}, m_{N_1} and m_{N_2}. Bottom panels: same, but for ϵ_2.

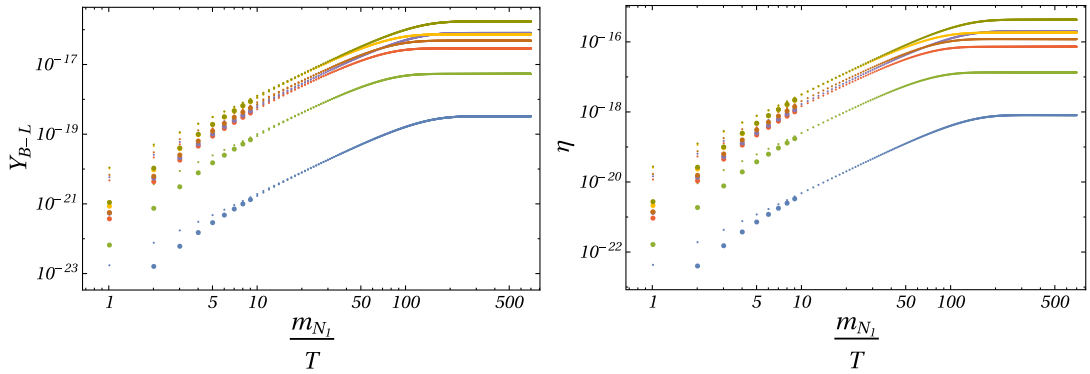

FIG. 6. The lepton asymmetry, Y_{B-L} (left) and the baryon asymmetry, η (right) versus $z = \frac{m_{N_1}}{T}$ corresponding to real κ for the set of selected parameter values as given in Table IV.

couplings (κ) on the *CP* asymmetries ϵ_1 and ϵ_2. We then the generated baryon asymmetry to determine if each scenario is compatible with the experimental data.

The scans are performed over the mass and coupling parameters in the range specified in Table III for each scenario. We now consider specific cases with κ_{1j} taken to be real, purely imaginary or complex and perform separate s for each case.

A. Case 1: Real positive κ

If κ is constrained to be real and positive, varying the right-handed neutrino masses, a scan will reveal the effects of the masses of right-handed neutrinos as well as of κ_{1j}. Here the mass of the lightest right-handed neutrino, m_{N_1}, is varied from 10 TeV to 100 TeV; the mass m_{N_2} is varied from 10^3 TeV to 10^4 TeV and the mass m_{N_3} is varied from 10^5 TeV to 10^6 TeV. The parameters ϵ_1 and ϵ_2 depend only on κ_{11}, κ_{12}, and κ_{13}. In this case, the vertex correction does not contribute to ϵ_2, and thus the *CP* asymmetry is dominated by ϵ^{sS} as in Eq. (5.9). In the standard channel, the influence of S to the self-energy correction will also be

TABLE IV. Parameter values for the Y_{B-L} and η plots in Fig. 6. The values of Y_{B-L} and η corresponding to these parameters are $Y_{B-L} \in (10^{-19}$–$10^{-16})$ and $\eta \in (10^{-18}$–$10^{-15})$.

κ_{11}	κ_{12}	m_{N_1} (TeV)	m_{N_2} (TeV)
0.024	0.097	29.8	6937.1
0.028	0.071	49.8	5802.6
0.025	0.071	61.9	4564.2
0.097	0.086	83.7	7585.8
0.013	0.087	19.6	7373.1
0.022	0.090	75.8	1459.1
0.025	0.022	19.8	7849.5
0.026	0.008	88.6	1060.7
0.031	0.008	11.3	8482.2
0.025	0.090	73.3	7837.5

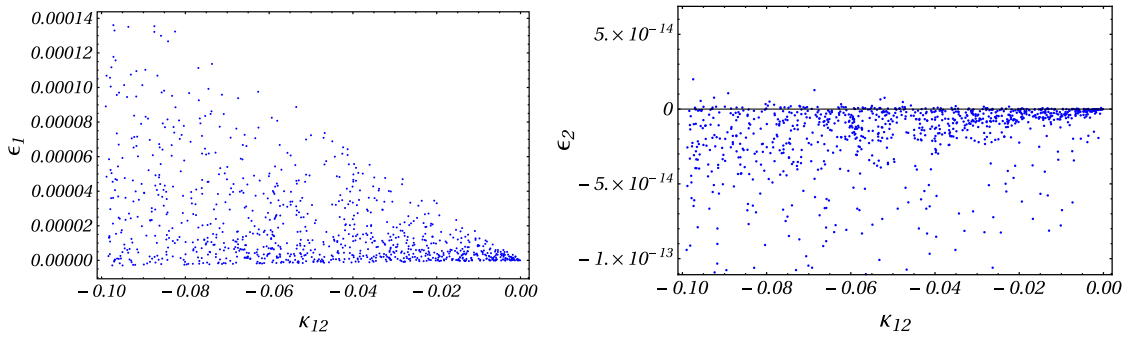

FIG. 7. *CP*-asymmetry parameters ϵ_1 (left) and ϵ_2 (right) versus κ_{12} for Case 2, for real negative κ values and right-handed neutrino masses, m_{N_j}, in a range as given in Table III.

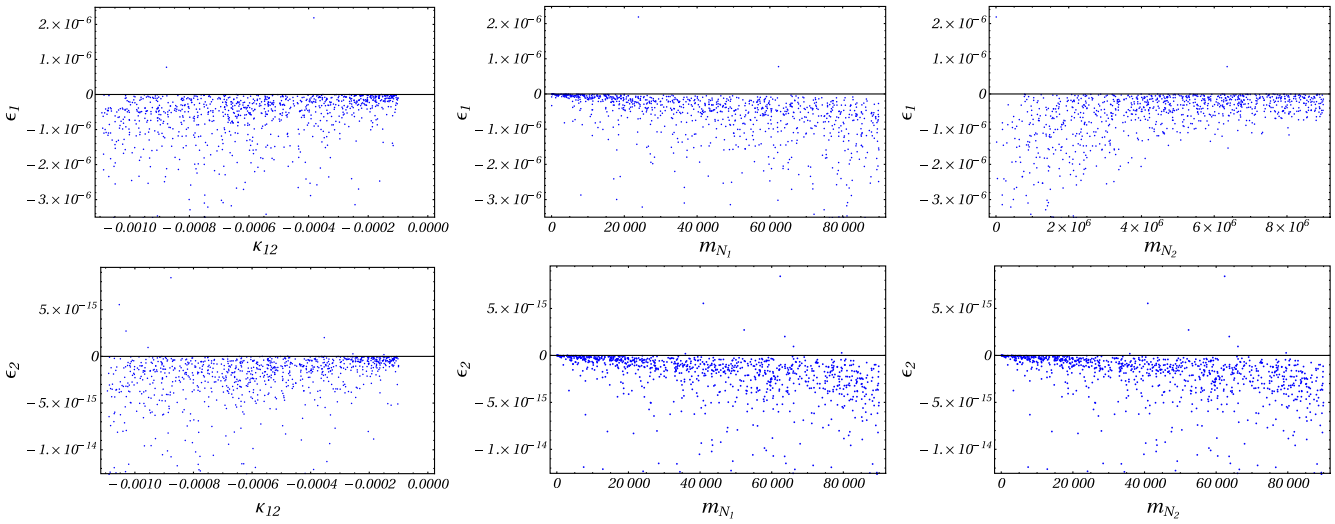

FIG. 8. *CP* asymmetry against the relevant coupling combination κ_{12} (left panels) and right-handed neutrino masses, m_{N_1} (middle panel)s and m_{N_2} (right panels) for ϵ_1 (top panels) and ϵ_2 (bottom panels), for Case 3, with imaginary values for κ_{12}.

affected by κ_{12} being real, as in Eq. (5.7). The efficiency factors ζ_1 and ζ_2 depend on the mass of right-handed neutrinos. Since ϵ_1 and ϵ_2 depend more sensitively on κ_{12} than on any other κ_{ij}'s, we focus on variations with κ_{12}. in Fig. 5 we show the dependence of ϵ_1 and ϵ_2 on κ_{12} and on the masses m_{N_1} and m_{N_2}. We note that throughout, varying the right-handed neutrino masses, ϵ_1 remains negative, while ϵ_2 is small and positive, showing that this is a robust prediction of real positive values of κ. The *CP* asymmetry parameter ϵ_2 is very small due to its inverse dependence on

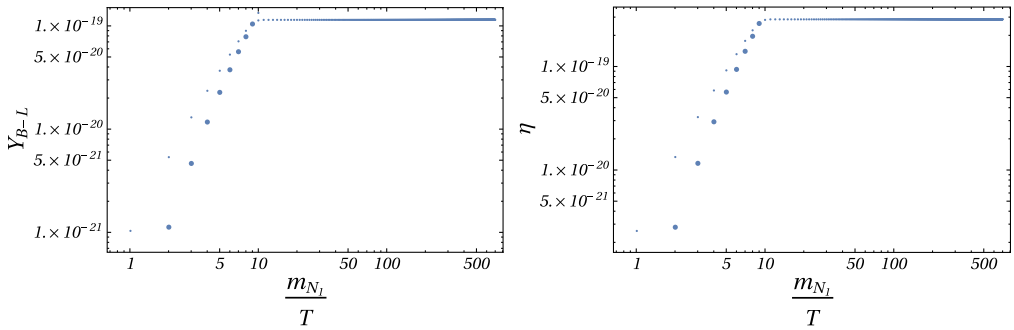

FIG. 9. The lepton asymmetry, Y_{B-L} (left) and the baryon asymmetry, η (right) versus $z = \frac{m_{N_1}}{T}$ corresponding to imaginary κ with parameter values as in Table V.

TABLE V. Parameter values for the Y_{B-L} and η plots in Fig. 9.

κ_{11}	κ_{12}	m_{N_1} (TeV)	m_{N_2} (TeV)
0.085	$-0.00063\imath$	41.9	3205.6
0.026	$-0.00076\imath$	16.4	1464.6

κ_{11}, which is orders of magnitude larger than K_{11}, while ϵ_1 is of order 10^{-5}. To further elucidate the resulting baryon asymmetry generated in this case, in Fig. 6 we plot the lepton asymmetry and the corresponding generated baryon asymmetry η against $z = \frac{m_{N_1}}{T}$ for a selected set of parameter values, as given in Table IV. Clearly, the baryon-antibaryon asymmetry obtained is many orders of magnitude smaller than the value required to generate the observed matter-antimatter asymmetry.

B. Case 2: Real negative κ

For negative values of κ_{1j}, the standard channel yields positive contributions (ϵ_1) to the CP asymmetry, while the contributions due to the new channels (ϵ_2) are negative, as is clear from Eqs. (5.7) and (5.9). These are plotted in Fig. 7. However, with ϵ_2 being many orders smaller than ϵ_1, the overall effect is such that the sign of η is negative, indicating a nonacceptable case of excess of antibaryons. Note however that the sign prediction for ϵ_1 is not robust. Due to the large uncertainty in the measurement of δ_{CP} (Eq. (5.5), the sign of K_{12} is flipped for the lower range of δ_{CP} compared to the central value and upper range. In particular, if we consider $\delta_{CP} < 180°$, we can obtain the desired sign for ϵ_1. However, even in that case, the numerical values for the CP asymmetry are found to be far too small to provide the required leptogenesis.

C. Case 3: Imaginary κ

We consider next the case where κ_{12} and κ_{13} are purely imaginary. The imaginary part of K_{12} plays the role of the phase factor for real positive κ_{12} and real negative κ_{12}, but in this case the real part of K_{12} also contributes to the asymmetry. The order of the real and imaginary parts of K_{12} are approximately same. Unlike the case where κ_{12} was real, here ϵ_1 and ϵ_2 have the same sign, meaning that their numerical values are negative for imaginary values of κ_{12} and κ_{13}. The numerical values of ϵ_2 are very small in comparison to ϵ_1, so ϵ_1 and the efficiency factor ζ_1 are not able to give required matter-antimatter asymmetry, as shown below. Varying neutrino masses populates the plot of ϵ_1 versus κ_{12} for ϵ_1 values closer to 0, while affecting ϵ_2 somewhat less significantly. The variations of ϵ_1 and ϵ_2 with κ_{12} and the masses, m_{N_1} and m_{N_2}, are shown in Fig. 8. Investigating the lepton number asymmetry generated in this case, sample points from across the parameter region considered could not provide the required baryon asymmetry. In Fig. 9 we show the evolution of Y_{B-L} and η for a couple of selected sets of parameter values, as given in Table V, to illustrate this point.

D. Case 4: Complex κ

We now the case where κ_{12} has both real and imaginary parts. The parameters K_{12} and K_{13} are complex but K_{11} is real. The real part of κ_{12} contributes to the asymmetry, together with the combination of the imaginary part of K_{12}, the imaginary part of κ_{12}, along with the real part of K_{12}. There are two phases in this case; one in the coupling constant Y_N and another in κ_{12}. We find that ϵ_1 and ϵ_2 can both acquire negative numerical values for complex κ_{12} and κ_{13}. More importantly, the numerical values of ϵ_2 and ϵ_1 are

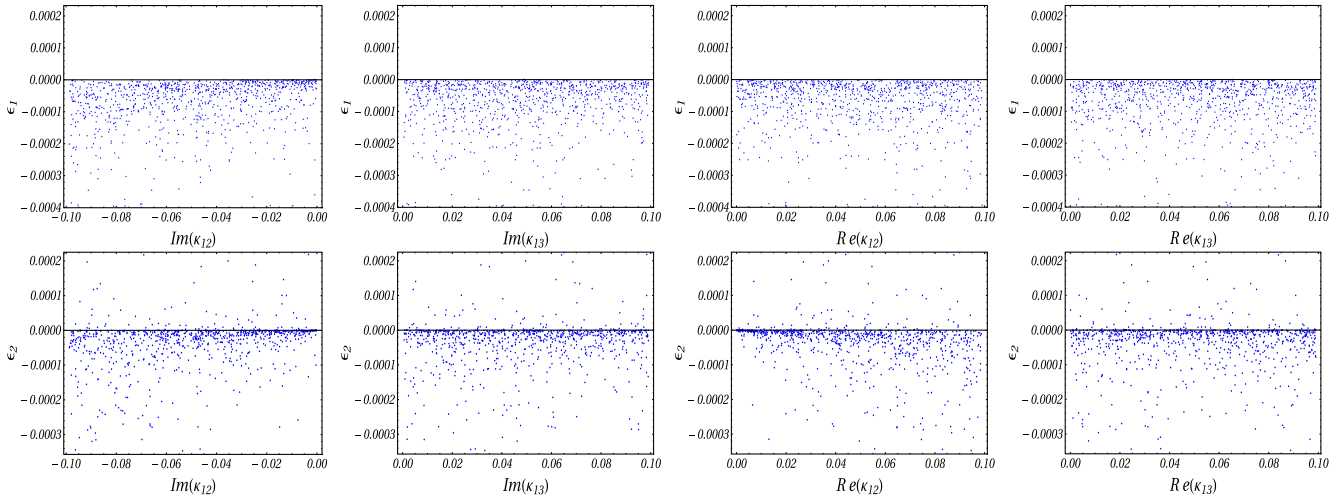

FIG. 10. CP asymmetry ϵ_1 (top panels) and ϵ_2 (bottom panels) plotted against the real and imaginary parts of the relevant coupling combination for Case 4, with complex κ and varying m_{N_j}. We show the dependence on $\mathrm{Im}\,\kappa_{12}$ (left panels), $\mathrm{Im}\,\kappa_{13}$ (left middle panels), $\mathrm{Re}\,\kappa_{12}$ (right middle panels) and $\mathrm{Re}\,\kappa_{13}$ (right panels).

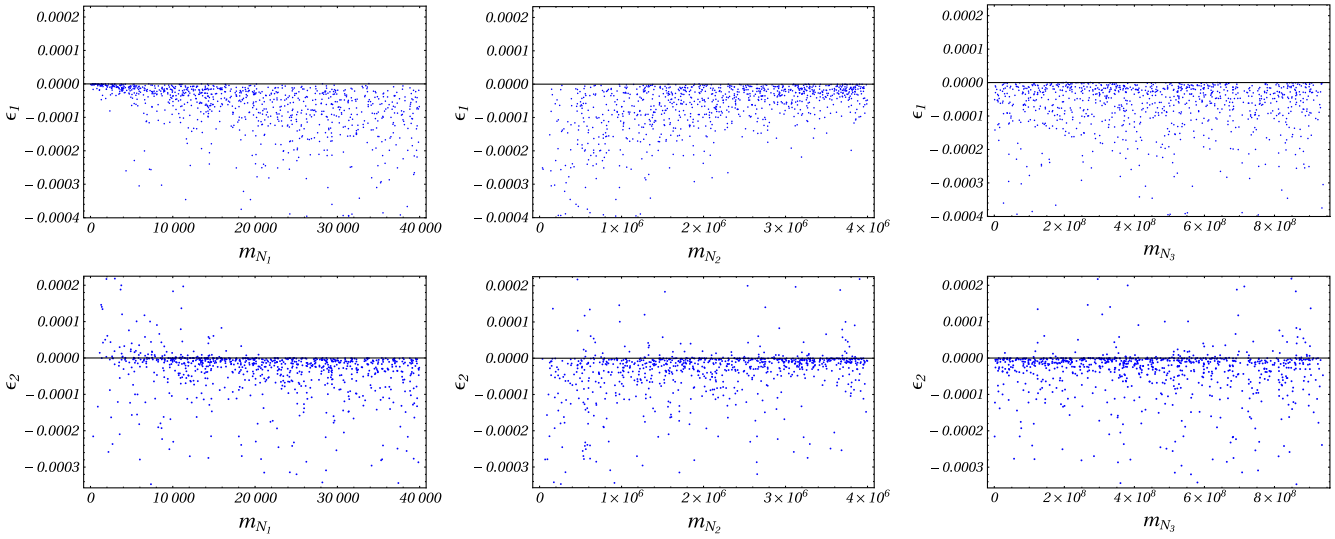

FIG. 11. *CP* asymmetry ϵ_1 (top panels) and ϵ_2 (bottom panels) plotted against the masses, m_{N_1} (left panels), m_{N_2} (middle panels) and m_{N_3} (right panels), for Case 4, with complex κ.

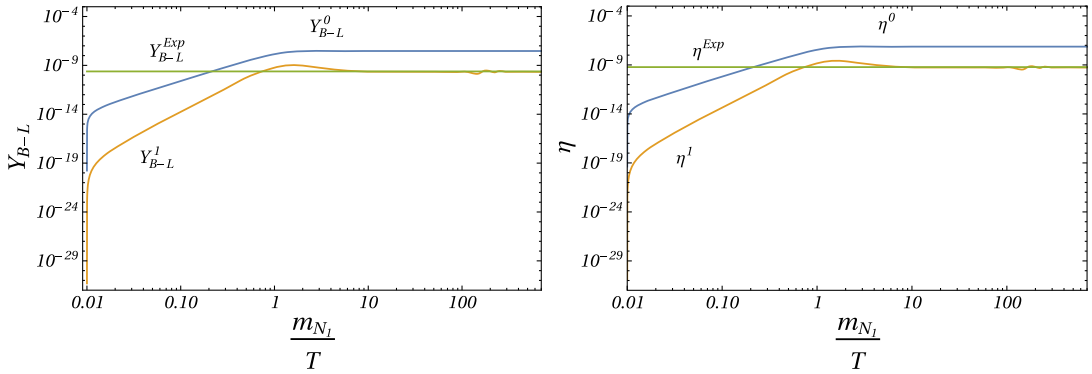

FIG. 12. The lepton asymmetry, Y_{B-L} (left) and the baryon asymmetry, η (right) versus $z = \frac{m_{N_1}}{T}$ for the case with complex κ and $m_{N_1} = 10$ TeV, $m_{N_2} = 10^3$ TeV, $\kappa_{13} = 10^{-1}, \kappa_{12} = 2(1-\imath)10^{-3}$. The superscripts 0 and 1 correspond to the cases without and with the washout terms induced by the scattering processes, respectively.

of the same order. In Fig. 10 we plot the dependence of ϵ_1 (top panels) and ϵ_2 (bottom panels) with the parameter κ_{12} and κ_{13}, separately for their real and imaginary parts, while in Fig. 11 we plot the dependence of ϵ_1 and ϵ_2 on the relevant right-handed neutrino masses m_{N_1}, m_{N_2} and m_{N_3}. We observe that by varying neutrino masses, regions of ϵ_1 negative and close to zero are evenly populated, while ϵ_2 is allowed to be positive. Note the similarities between the dependence of ϵ_1 and ϵ_2 on $\mathrm{Re}\,\kappa_{12}$ and $\mathrm{Re}\,\kappa_{13}$; while the plots for ϵ_2 versus $\mathrm{Im}\,\kappa_{12}$ and $\mathrm{Im}\,\kappa_{13}$ favor values close to zero, the variation of ϵ_1 on the same parameters is slightly different.

To study the asymmetry, in this case in Fig. 12 we plot the dependence of the lepton asymmetry, Y_{B-L} (left) and the baryon asymmetry, η (right), with $z = \frac{m_{N_1}}{T}$ for the case with complex κ for a representative set of parameter values, as indicated in the caption. One can see that, unlike scenarios where we consider κ_{12} purely real or purely imaginary, this case is compatible with the requirement of yielding sufficient baryon asymmetry in the Universe.

TABLE VI. Benchmark point for the comparison of standard leptogenesis case with the new scenario.

m_{N_1} (TeV)	m_{N_2} (TeV)	m_{N_3} (TeV)	m_χ (GeV)	m_ψ (GeV)	m_S (GeV)	κ_{11}	κ_{12}	κ_{13}
10	1020	8.76×10^5	200	60	175	0.018	$(2 + .055\imath) \times 10^{-3}$	$(4.51 - 5.5\imath) \times 10^{-4}$

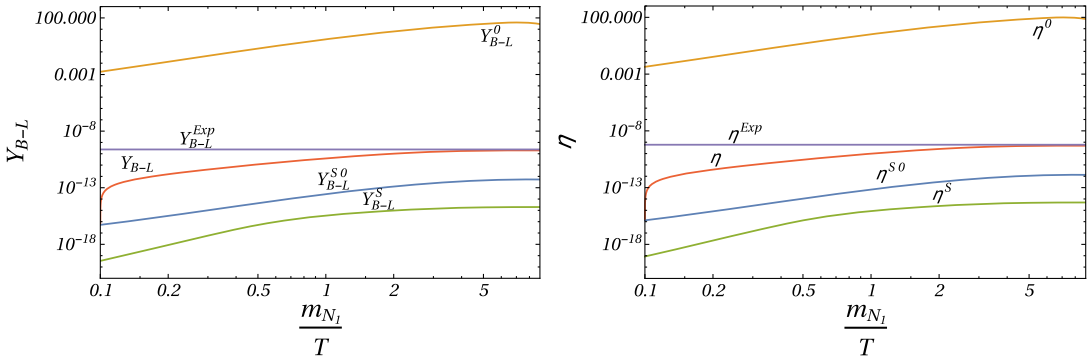

FIG. 13. Plot for Y_{B-L} and η showing the contribution of the standard leptogenesis and the total contribution in the new scenario for the benchmark point given in Table VI. (Left panel): the lepton asymmetry Y_{B-L}. (Right panel): the induced baryon asymmetry η. Here the superscript S indicates the standard contribution, while superscripts 0 and 1 represent contributions without and with scattering, respectively.

E. Comparison of the standard leptogenesis with the new model effects

In the previous subsections we showed that, with suitably chosen parameter values, our model could explain the observed baryon asymmetry of the Universe. The presence of the new charged scalar that interacts directly with the right-handed neutrinos boosts the CP asymmetry, inducing the required baryon asymmetry. We further illustrate this by comparing the standard leptogenesis case (in the absence of the new degrees of freedom) with the scenario considered here, including all possibilities described above. To highlight the differences, we fix the mass of the lightest right-handed neutrino to be $m_{N_1} = 10$ TeV, and other masses and relevant parameter values as given in Table VI. Choosing m_{N_1} so light means sufficient leptogenesis cannot be generated in seesaw Type-I models without neutrino mass degeneracy, whereas in our model there is an additional channel that violates lepton number in the decay process, and both channels are important in the analysis. Numerical solutions of Boltzmann equations for this case are plotted in Fig. 13, giving the evolution of the lepton asymmetry and the corresponding induced baryon asymmetry. The left side plot shows the lepton asymmetry Y_{B-L}, with curves labeled Y^{S0}_{B-L} and Y^{S}_{B-L} representing the yields in the standard case without and with the washout effects induced by scattering included, respectively, and Y^{0}_{B-L} and Y_{B-L}, respectively, representing the total yields including the new contributions. The curve $Y^{\rm Exp}_{B-L}$ represents the lepton asymmetry needed to generate the correct matter-antimatter asymmetry. Similarly, in the right side plot, η^0 and η^{S0} correspond to the standard contribution alone without and with scattering effects, respectively, and the top curves η^0 and η correspond to the total contribution in our model, without and with the effects of washout scattering processes. The flat curve labeled $\eta^{\rm Exp}$ represents the observed baryon asymmetry. These plots show that while standard leptogenesis alone is unable to generate required matter-antimatter asymmetry at low masses, the addition of the new degrees of freedom makes up the deficit.

VI. CONCLUSION

In this work we presented the analysis of a simple extension of the SM to account for both a dark matter candidate and a mechanism for leptogenesis which could produce sufficient asymmetry to generate the matter-antimatter discrepancy in the Universe. The extension includes, in addition to three Majorana right-handed neutrinos, a gauge singlet charged scalar field S^+, plus a charged (χ^+) and a neutral (ψ) singlet fermions, with the latter two are odd under an additional Z_2 symmetry. In this scenario, ψ is a stable dark matter candidate, interacting with the other particles through its Yukawa coupling alone. When this coupling is very small, the abundance of dark matter is due to the slow two-body decay of $\chi^+ \to S^+\psi$, if kinematically allowed, or the four-body decay $\chi^+ \to \phi\ell\nu\psi$, in the regions where the two-body decay is forbidden. We implement the freeze-in mechanism and show that, for a wide range of masses and couplings, the relic abundance is consistent with the experimental data. We then this parameter space to find regions favorable to decays of heavy right-handed neutrinos into leptons (or antileptons) plus doublet Higgs bosons (standard leptogenesis), or into the new charged scalar S^+ and leptons or antileptons (new contributions). Leptogenesis is generated by the CP-violating interference between the tree-level process and one-loop contributions from self-energy and vertex corrections, facilitated by the nonequilibrium conditions when the temperature of the Universe is of the same order as the mass of the decaying heavy neutrino.

The canonical thermal leptogenesis with hierarchal right-handed neutrinos requires them to be very heavy to generate the required baryon asymmetry, unless at least two of them are closely degenerate. In our model, additional possibilities open through the Yukawa interaction of the new charged scalar S. Due to the influence of the new

scalar particle, in addition to the standard decay channel, $N \to \phi\ell$, a new decay channel, $N \to S\ell$ opens up, contributing to the lepton number asymmetry. Considering the Boltzmann evolution equations in the present scenario, a detailed analysis of the parameter space was performed. The CP parameters ϵ_1 and ϵ_2 depend on the coupling constants of the heavy neutrinos with the Higgs boson (Y_N) and with the new charged scalar S (y_2), where the former is constrained by light neutrino masses and mixings, while the latter is largely unconstrained. Denoting the relevant combination that enter the CP asymmetry as $K_{ij} = (Y_N^\dagger Y_N)_{ij}$ and $\kappa_{ij} = (y_2^\dagger y_2)_{ij}$, we studied different cases with κ taken to be real, purely imaginary, or complex, leading to the results broadly summarized as below.

(i) For the real κ case only the imaginary K_{12} contributes to the CP asymmetry, while the real part of K_{12} contributes to CP asymmetry for imaginary values of κ, whereas in the case of complex κ_{12} both the real and the imaginary parts of K_{12} contribute to the CP asymmetry. Note that, the real and the imaginary parts of K_{12} are both of the same order.

(ii) For the case of complex κ, the required leptogenesis can be generated for $m_{N_1} = 10$ TeV, while the other two cases with real κ or imaginary κ are found to be inadequate in generating it for the entire allowed range of parameter space.

In conclusion, we have shown that a simple, minimally extended SM scenario, can account for both dark matter though the freeze-in mechanism, and provide sufficient CP asymmetry through leptogenesis. This mechanism is capable of generating the required matter antimatter asymmetry for relatively light right-handed neutrino masses (10 TeV) without resorting to resonant leptogenesis. We explicitly have shown that the same parameter region is compatible with the observed dark matter relic abundance with the dark matter and the associated particles in the sub-TeV mass range.

ACKNOWLEDGMENTS

The work of M. F. has been partly supported by Natural Sciences and Engineering Research Council of Canada through Grant No. SAP105354.

[1] N. Aghanim *et al.* (Planck Collaboration), Astron. Astrophys. **641**, A5 (2020).
[2] S. Burles, K. M. Nollett, and M. S. Turner, Nucl. Phys. **A663**, 861c (2000).
[3] A. D. Sakharov, Usp. Fiz. Nauk **161**, 61 (1991) [Sov. Phys. Usp. **34**, 392 (1991)].
[4] V. A. Kuzmin, V. A. Rubakov, and M. E. Shaposhnikov, Phys. Lett. **155B**, 36 (1985).
[5] V. A. Rubakov and M. E. Shaposhnikov, Usp. Fiz. Nauk **166**, 493 (1996).
[6] A. D. Dolgov, Phys. Rep. **222**, 309 (1992).
[7] M. Dine, P. Huet, and R. L. Singleton, Jr., Nucl. Phys. **B375**, 625 (1992).
[8] M. Dine, R. G. Leigh, P. Huet, A. Linde, and D. Linde, Phys. Rev. D **46**, 550 (1992).
[9] V. Jain and A. Papadopoulos, Phys. Lett. B **303**, 315 (1993).
[10] J. Espinosa, M. Quirós, and F. Zwirner, Phys. Lett. B **314**, 206 (1993).
[11] M. Fukugita and T. Yanagida, Phys. Lett. B **174**, 45 (1986).
[12] J. A. Harvey and M. S. Turner, Phys. Rev. D **42**, 3344 (1990).
[13] M. Luty, Phys. Rev. D **45**, 455 (1992).
[14] L. Covi, E. Roulet, and F. Vissani, Phys. Lett. B **384**, 169 (1996).
[15] R. Barbieri, P. Creminelli, A. Strumia, and N. Tetradis, Nucl. Phys. **B575**, 61 (2000).
[16] S. Davidson and A. Ibarra, Phys. Lett. B **535**, 25 (2002).
[17] W. Buchmuller, P. Di Bari, and M. Plumacher, Nucl. Phys. **B643**, 367 (2002); **B793**, 362(E) (2008).
[18] G. F. Giudice, A. Notari, M. Raidal, A. Riotto, and A. Strumia, Nucl. Phys. **B685**, 89 (2004).
[19] W. Buchmuller, P. Di Bari, and M. Plumacher, Ann. Phys. (Amsterdam) **315**, 305 (2005).
[20] W. Buchmuller, R. Peccei, and T. Yanagida, Annu. Rev. Nucl. Part. Sci. **55**, 311 (2005).
[21] K. Petraki and A. Kusenko, Phys. Rev. D **77**, 065014 (2008).
[22] S. Davidson, E. Nardi, and Y. Nir, Phys. Rep. **466**, 105 (2008).
[23] M. Frigerio, T. Hambye, and E. Ma, J. Cosmol. Astropart. Phys. 09 (2006) 009.
[24] S. Pascoli, S. T. Petcov, and A. Riotto, Nucl. Phys. **B774**, 1 (2007).
[25] S. Pascoli, S. T. Petcov, and A. Riotto, Phys. Rev. D **75**, 083511 (2007).
[26] A. De Simone and A. Riotto, J. Cosmol. Astropart. Phys. 08 (2007) 002.
[27] H. An, S.-L. Chen, R. N. Mohapatra, and Y. Zhang, J. High Energy Phys. 03 (2010) 124.
[28] A. Falkowski, J. T. Ruderman, and T. Volansky, J. High Energy Phys. 05 (2011) 106.
[29] M. Drewes and B. Garbrecht, J. High Energy Phys. 03 (2013) 096.
[30] C. S. Fong, E. Nardi, and A. Riotto, Adv. High Energy Phys. **2012**, 158303 (2012).
[31] N. Bernal, M. Heikinheimo, T. Tenkanen, K. Tuominen, and V. Vaskonen, Int. J. Mod. Phys. A **32**, 1730023 (2017).
[32] A. Pilaftsis and T. E. Underwood, Nucl. Phys. **B692**, 303 (2004).

[33] A. Pilaftsis and T. E. J. Underwood, Phys. Rev. D **72**, 113001 (2005).
[34] D. Aristizabal Sierra, M. Losada, and E. Nardi, Phys. Lett. B **659**, 328 (2008).
[35] M. Le Dall and A. Ritz, Phys. Rev. D **90**, 096002 (2014).
[36] P. Hernández, M. Kekic, J. López-Pavón, J. Racker, and N. Rius, J. High Energy Phys. 10 (2015) 067.
[37] T. Hambye, F. S. Ling, L. Lopez Honorez, and J. Rocher, J. High Energy Phys. 07 (2009) 090; 05 (2010) 066(E).
[38] T. Alanne, T. Hugle, M. Platscher, and K. Schmitz, J. Cosmol. Astropart. Phys. 03 (2019) 037.
[39] A. Abada, G. Arcadi, V. Domcke, M. Drewes, J. Klaric, and M. Lucente, J. High Energy Phys. 01 (2019) 164.
[40] M. Drewes, B. Garbrecht, D. Gueter, and J. Klaric, J. High Energy Phys. 08 (2017) 018.
[41] J. Klarić, M. Shaposhnikov, and I. Timiryasov, Phys. Rev. D **104**, 055010 (2021).
[42] Y. Abe, T. Ito, and K. Yoshioka, arXiv:2110.11096.
[43] D. Borah, A. Dasgupta, S. Mahapatra, and N. Sahu, arXiv:2112.14786.
[44] T. P. Walker, G. Steigman, D. N. Schramm, K. A. Olive, and H.-S. Kang, Astrophys. J. **376**, 51 (1991).
[45] B. D. Fields, K. A. Olive, T.-H. Yeh, and C. Young, J. Cosmol. Astropart. Phys. 03 (2020) 010; 11 (2020) E02.
[46] S. S. McGaugh, J. M. Schombert, W. J. G. de Blok, and M. J. Zagursky, Astrophys. J. Lett. **708**, L14 (2010).
[47] R. H. Cyburt, B. D. Fields, and K. A. Olive, Astropart. Phys. **17**, 87 (2002).
[48] M. Bauer and T. Plehn, *Yet Another Introduction to Dark Matter*, Lecture Notes in Physics (Springer, Cham, 2019), p. 959.
[49] N. Aghanim *et al.* (Planck Collaboration), Astron. Astrophys. **641**, A6 (2020).
[50] J. Billard *et al.*, Rep. Prog. Phys. **85**, 056201 (2022).
[51] J. McDonald, Phys. Rev. Lett. **88**, 091304 (2002).
[52] L. J. Hall, K. Jedamzik, J. March-Russell, and S. M. West, J. High Energy Phys. 03 (2010) 080.
[53] G. Bélanger *et al.*, J. High Energy Phys. 02 (2019) 186.
[54] M. Klasen and C. E. Yaguna, J. Cosmol. Astropart. Phys. 11 (2013) 039.
[55] F. Elahi, C. Kolda, and J. Unwin, J. High Energy Phys. 03 (2015) 048.
[56] R. T. Co, F. D'Eramo, L. J. Hall, and D. Pappadopulo, J. Cosmol. Astropart. Phys. 12 (2015) 024.
[57] A. Goudelis, P. Papachristou, and V. C. Spanos, Phys. Rev. D **105**, 043521 (2022).
[58] L. J. Hall, J. March-Russell, and S. M. West, arXiv: 1010.0245.
[59] S. Chakraborti, V. Martin, and P. Poulose, J. Cosmol. Astropart. Phys. 03 (2020) 057.
[60] R. N. Mohapatra and G. Senjanovic, Phys. Rev. Lett. **44**, 912 (1980).
[61] R. N. Mohapatra and G. Senjanovic, Phys. Rev. D **23**, 165 (1981).
[62] J. Schechter and J. W. F. Valle, Phys. Rev. D **22**, 2227 (1980).
[63] P. Minkowski, Phys. Lett. **67B**, 421 (1977).
[64] S. L. Glashow, NATO Sci. Ser. B **61**, 687 (1980).
[65] M. Gell-Mann, P. Ramond, and R. Slansky, Conf. Proc. **C790927**, 315 (1979).
[66] P. A. Zyla *et al.* (Particle Data Group), Prog. Theor. Exp. Phys. **2020**, 083C01 (2020).
[67] Z.-z. Xing, Chin. Phys. C **34**, 1 (2010).
[68] J. A. Casas and A. Ibarra, Nucl. Phys. **B618**, 171 (2001).
[69] I. Esteban, M. C. Gonzalez-Garcia, M. Maltoni, T. Schwetz, and A. Zhou, J. High Energy Phys. 09 (2020) 178.